Sequence-Dependent Surface Coverage of ssDNA coatings on Single-Wall Carbon Nanotubes

Ali A. Alizadehmojarad[†§], Sergei M. Bachilo[†], and R. Bruce Weisman[*,†,‡]

[†] Department of Chemistry and the Smalley-Curl Institute, Rice University, Houston, TX 77005 United States

[‡] Department of Materials Science and NanoEngineering, Rice University, Houston, TX 77005 United States

[§] Present address: Department of Chemical Engineering, Massachusetts Institute of Technology, Cambridge, MA 02139 United States

Abstract

A combination of experimental measurements and molecular dynamics (MD) simulations was used to investigate how the surfaces of single-wall carbon nanotubes (SWCNTs) are covered by adsorbed ssDNA oligos with different base compositions and lengths. By analyzing the UV absorption spectra of ssDNA-coated SWCNTs before and after coating displacement by a transparent surfactant, the mass ratios of adsorbed ssDNA to SWCNTs were determined for poly-T, poly-C, GT-containing, and AT-containing ssDNA oligos. Based on the measured mass ratios, it is estimated that an average of 20, 22, 26, or 32 carbon atoms are covered by one adsorbed thymine, cytosine, adenine, or guanine nucleotide, respectively. In addition, the UV spectra revealed electronic interactions of varying strengths between the nucleobase aromatic rings and the nanotube π-systems. Short poly-T DNA oligos show stronger π–π stacking interactions with SWCNT surfaces than do short poly-C DNA oligos, whereas both long poly-C and poly-T DNA oligos show strong interactions. These experiments were complemented by MD computations on simulated systems that were constrained to match the measured ssDNA/SWCNT mass ratios. The surface coverages computed from the MD results varied with oligo composition in a pattern that correlates higher measured yields of nanotube fluorescence with greater surface coverage.

Keywords: ssDNA adsorption; nanotube surfactants, molecular dynamics simulation, experimentally guided MD

INTRODUCTION

Single-wall carbon nanotubes (SWCNTs) are synthetic nanomaterials consisting of carbon atoms covalently linked to form tubular structures with large aspect ratios.[1] SWCNTs exist in a variety of structural forms that display a range of electronic, optical, physical, and chemical properties. These structural species differ in their diameters and roll-up (chiral) angles, with each one uniquely labeled by a pair of integers, its (*n*,*m*) indices.[2] Many studies and applications of SWCNTs rely on their dispersion in aqueous solution with the aid of surfactant or polymeric coatings.[3,4] Previous experimental studies have suggested that the noncovalent interactions between nanotubes and coatings may depend on factors that include charge density, surface coverage, packing density, and mass ratio.[5–9] Computational simulations have also provided important insights into the structures and interactions of SWCNT coatings.[9–15]

A particularly interesting coating is single-stranded DNA (ssDNA),[16] because it has been found that some noncovalent interactions between SWCNTs and short ssDNA oligos depend on both the specific (*n*,*m*) species and specific ssDNA base sequence.[17–21] This recognition effect has been applied to achieve highly selective structural sorting of SWCNT mixtures.[17,19,22–25] Although the structures of simple surfactant coatings on SWCNTs have been studied using combined experimental and computational methods,[26] similar investigations of ssDNA coatings are lacking. Even in the absence of specific recognition between the ssDNA oligo and the SWCNT species, such research is challenging because the adsorbed morphologies are not yet clear and may depend on the length and base sequence of the ssDNA oligo and also on the structure of the SWCNT.[11,26–30] One experimental measurement that can be used to guide molecular dynamics (MD) simulations is the coating-to-nanotube mass ratio. Another is the relative quantum yield of SWCNT fluorescence, which reflects the extent to which the coating shields the nanotube surface from its aqueous environment and reduces external quenching of excitons.[31] We report here a combined experimental and computational study that explores the effects of oligo length and composition through measurements of ssDNA-to-SWCNT mass ratios and the use of those ratios in constrained MD simulations of several ssDNA oligos interacting with SWCNTs of different diameters.

METHODS

General approach

Absorption spectroscopy is one of the most common methods for determining solute concentrations. SWCNT dispersions containing metallic and semiconducting SWCNTs absorb light from the ultraviolet (UV) to near-infrared (NIR) regions due to transitions of their extended π-electron systems. Although the NIR absorptions of different semiconducting SWCNT species are relatively sharp and distinct, their UV absorptions overlap enough to allow simple measurement of the total metallic plus semiconducting SWCNT concentration, as described in our recent study.[26] The concentrations of ssDNA oligos with known base sequences can readily be quantified from UV absorption spectra by applying the known absorptivity values arising from their pyridine and purine base contents. After dialysis has been used to remove free ssDNA from dispersed samples, UV absorption spectroscopy should thus allow measurement of the ssDNA-to-SWCNT ratios of suspended nanotubes. However, a complicating factor is electronic coupling between the physisorbed ssDNA bases and the SWCNT π-system, which makes UV spectra deviate substantially from simple linear combinations of the two separate components. We address this issue by adding sufficient SDS surfactant to displace all ssDNA from the nanotube surfaces, restoring the system's spectrum to an easily analyzed superposition of components from free ssDNA and SDS-coated SWCNTs. The added SDS does not interfere because is transparent in the UV region of interest. After spectroscopically finding the ssDNA-to-SWCNT mass ratios for various oligos, we use those results to constrain MD simulations that investigate how the ssDNA oligos cover SWCNT surfaces at the experimentally determined compositions.

Sample Preparation

All nanotube dispersions were prepared using SWCNTs grown in the Rice University HiPco reactor (batch 195.1). Custom-synthesized ssDNA oligos were purchased from Integrated DNA Technologies, Inc. (IDT). We mixed the ssDNA and SWCNTs in 0.1 M sodium chloride and 0.06 M sodium phosphate buffer (pH=7.4) at a DNA/SWCNT mass ratio of approximately 2 and tip-sonicated the mixture with a Branson digital sonifier (3 mm tip) at 6 W output power for 20 active minutes (cycles of 30 s off, 30 s on for 40 min). Undispersed SWCNTs and aggregates were then removed through two 90 min centrifugations (Biofuge-13, Baxter Scientific) at 13000 × g,

extracting 80% of the supernatant each time. The same phosphate buffer was used for diluting the sample and preparing stock solutions.

Spectroscopic sample characterization

We used a prototype model NS2 NanoSpectralyzer (Applied NanoFluorescence, LLC) to measure visible and NIR absorption spectra and NIR fluorescence spectra with excitation wavelengths of 642, 659, and 784 nm.[32,33] UV-vis absorption spectra were measured on a Cary 60 spectrophotometer (Agilent). Absorptivity values of our DNA oligos at 260 nm were provided by Integrated DNA Technologies, and the UV absorptivity of HiPco SWCNTs (batch 195.1) was taken from our recent report.[26] All measurements were made with samples in fused silica cuvettes with 1 cm optical path lengths.

Removing free DNA from the DNA-dispersed SWCNT samples

SWCNT dispersions in DNA contain both free and SWCNT-adsorbed DNA oligos. To remove the free or unbound DNAs, we dialyzed dispersions using 10 mL Spectra-Por Float-A-Lyzer G2 dialysis tubes (Spectrum Labs) with a molecular weight cutoff of 100 kDa. The dialysis membranes were not permeable to SWCNTs. Almost 6 mL of the stock solution of ssDNA-dispersed SWCNTs was loaded into a dialysis tube and immersed in 480 mL of fresh buffer. We dialyzed the samples twice, refreshing the buffer outside the dialysis tube every 24 h. NIR absorption, fluorescence, and UV absorption spectra of the samples were measured before and after dialysis to monitor the removal of free DNAs. Spectra of a representative SWCNT dispersion are presented in Figure S1. Figures S1a,b suggest a drop in NIR absorption while the fluorescence spectrum remained nearly the same after dialysis. This implies that non-emissive species had been removed during the dialysis treatment. More importantly, Figure S1c shows a significant decrease in UV absorption after dialysis, which we attribute mainly to the removal of free DNA oligos.

Molecular Dynamics Simulations

Experimental studies of DNA oligo conformations on the SWCNTs are very challenging. As an alternative, atomistic molecular dynamics (MD) simulations provide an indirect tool that we used to computationally investigate this multivariable problem. We simulated the wrapping of eight different ssDNA oligonucleotides, including T_{12}, T_{39}, C_{12}, C_{30}, $(GT)_6$, $(AAT)_4$ and $(AAAT)_3$, on (6,5), (7,6), or (8,7) SWCNTs (representing different diameters). For comparison, we also simulated SDS surfactant coatings on (6,5), (7,6) and (8,7) SWCNTs and studied surfactant

morphologies around SWCNTs. We simulated the solvation and charge neutralization (with 0.1 M NaCl for all simulations) of DNA-wrapped SWCNTs using the Solvate and Ionize VMD plugins. In case of SDS-coated SWCNTs, we used only sodium counter ions to neutralize the negative charges on the sulfate groups of SDS molecules. TIP3P and CHARMM36 force fields were used for describing water molecules and other species, respectively.[34] We performed all MD simulations with the NAMD 2.13 package[35] at a constant temperature of 300 K and constant pressure of 1 bar, consistent with experimental conditions, through Langevin dynamics with a Langevin constant of γ_{Lang}= 1.0 ps^{-1}. The particle mesh Ewald (PME) method[36] was used to evaluate Coulomb interactions while maintaining periodic boundary conditions in all directions. We performed 1000 steps of energy minimization and 2 ns of equilibration simulations prior to production runs lasting at least 100 ns. In all simulations, we placed three DNA strands around one nanotube segment. For studying DNA oligos with twelve nucleotides, the dimension of our simulation box was 4×4×16 nm^3 (containing ~7,000 water molecules). For T_{39}-wrapped (6,5) SWCNTs, the box was 4×4×30 nm^3 (~12,000 water molecules), and for T_{39}-wrapped (7,6) or (8,7) SWCNTs the box was 4×4×26 nm^3 (~10,000 water molecules). Simulations of C_{30}-wrapped (6,5) and (7,6) or (8,7) SWCNTs used solvation boxes of 4×4×28 nm^3 (~11,000 water molecules) and 4×4×22 nm^3 (8,600 water molecules), respectively. In each MD simulation, we selected a SWCNT segment length that, when wrapped by three ssDNA strands, matched our experimentally determined DNA/SWCNT mass ratio (see Supporting Information). For simulating SDS-coated SWCNTs, we used a 16 nm nanotube segment of (6,5), (7,6), or (8,7) SWCNTs in a 14×14×18 nm^3 box.

To estimate the length of SWCNTs covered by ssDNA oligos, we first found the axial separation between the two bases within a DNA strand giving the maximum end-to-end separation. That distance was then divided by the total SWCNT length in each MD simulation. SWCNT area coverage was computed by first computing the number of SWCNT carbon atoms covered by DNA or SDS molecules, based on our previously described procedure.[26] We then divided the number of covered SWCNT carbon atoms by the total number of SWCNT carbon atoms to obtain the SWCNT area coverage fraction. The ensemble averages of all these quantities were evaluated for the last 80 ns of the simulations. We also averaged these quantities over (6,5), (7,6), and (8,7) SWCNT chiralities to approximately represent experimental samples, because those species have

diameters roughly centered within the actual diameter distribution. Finally, as a separate estimate of coverage to compare with experimental reports, we performed MD simulations of single pyrimidine or pyridine nucleotides adsorbed on graphene flakes.

RESULTS AND DISCUSSION

Experiments

We selected a small set of ssDNA oligos to explore the effect of base sequence and length on their interactions with SWCNTs. T_{12}, T_{39}, C_{12}, and C_{30} let us compare oligos of different lengths containing only pyrimidine bases, and $(GT)_6$, $(AAT)_4$, and $(AAAT)_3$ represented 12-base oligos in the GT and AT families that are commonly used as SWCNT dispersants. The initial DNA/SWCNT mass ratio in all sample preparations was chosen to be 2, except for one dispersion (marked with an asterisk), where this ratio was 1 to check for the sensitivity of our results to the initial DNA concentration. Figure 1 shows the absorption and fluorescence spectra (with 642 nm excitation) of dispersions with the representative short DNA coatings C_{12}, T_{12}, $(AAT)_4$, and $(GT)_6$. The spectra of SWCNTs dispersed in the other DNA oligos, $(GT)_6^*$, $(AAAT)_3$, C_{30}, and T_{39}, are presented in the Supporting Information (Figure S1). Interactions between the π electrons of the nanotube surface and aromatic rings of the DNA bases cause significant perturbations of the samples' absorption and fluorescence spectra. As described previously,[26] our method involves removing these interactions to allow reliable spectrometric determinations of composition. We achieved this by adding SDS to displace the DNA oligos from the SWCNT surface, giving separated DNA and SWCNTs. The kinetic and thermodynamic aspects of such SWCNT coating displacements have previously been studied by several investigators using near-IR spectroscopies.[18,29,37–43] Here we performed UV absorption analysis to quantitate the SWCNT and ssDNA contents, exploiting the fact that the added SDS is a saturated compound that is transparent at the relevant UV wavelengths. In addition to observing the expected displacement-induced blue-shifts in SWCNT near-IR absorption and fluorescence peaks (Figures 1, S1), we measured the UV-vis absorption spectra of DNA-dispersed SWCNTs before and after adding SDS. These showed that the SWCNT UV absorption intensified after the π–π interactions with ssDNA were removed by coating displacement (Figures 2, S2). Moreover, although the measured UV absorption spectra of DNA-coated SWCNTs deviated markedly from linear combinations of free DNA and pristine SWCNT absorptions, such linear combinations precisely fit spectra of the same samples after displacement

by SDS (Figure S4 illustrates the component spectra and fits). We then were able to find the absolute concentrations of ssDNA and SWCNT in the dialyzed samples from the best fit coefficients of the two spectral basis functions, which were the quantitative UV absorptivity spectra of pristine SWCNTs in SDS[26] and of free ssDNAs.

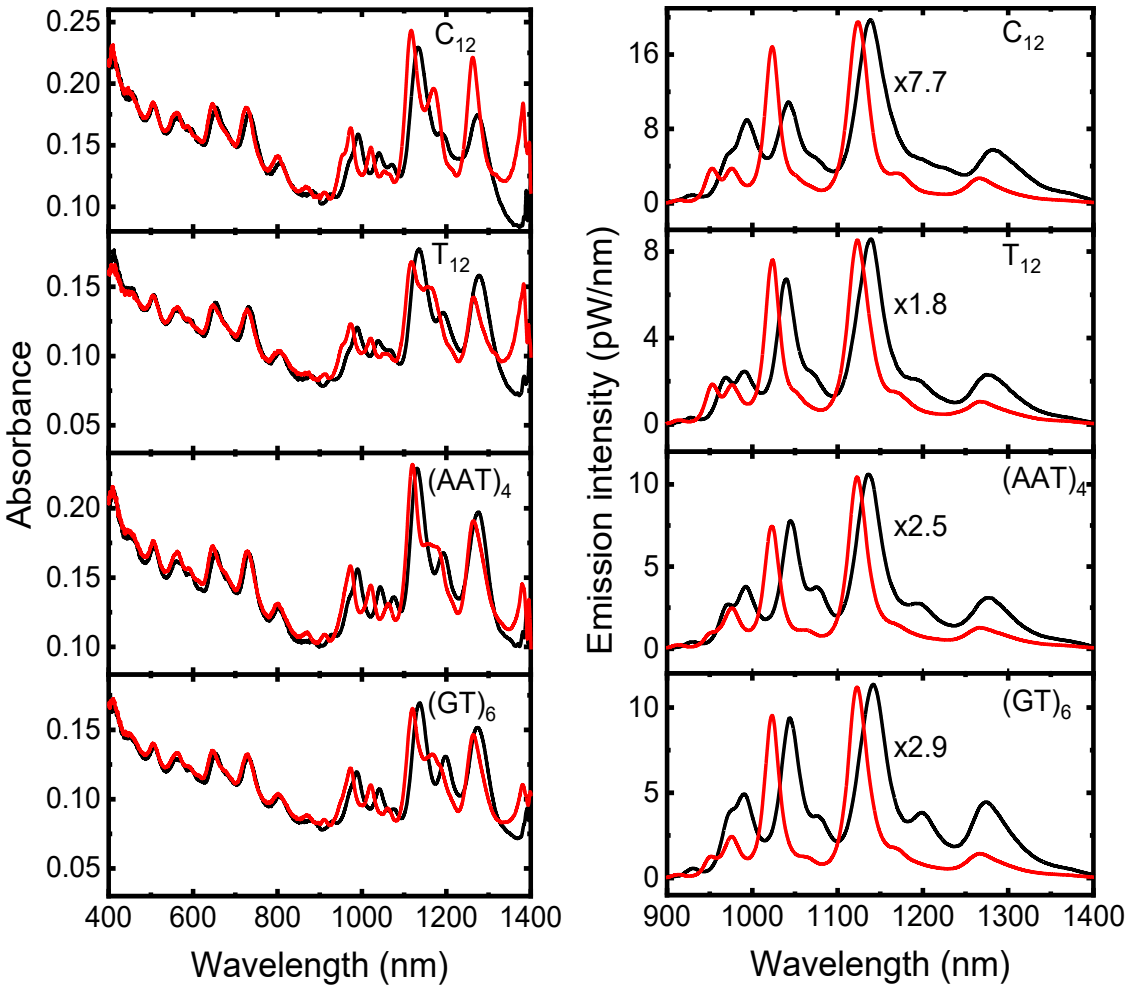

Figure 1. Absorption and emission spectra of 195.1 HiPco SWCNTs dispersed in four different ssDNA oligos, as labeled in the frames. The left and right stacked plots display the absorption and emission spectra, respectively. Curves show the spectra before (black) and after (red) displacement of the DNA coatings by SDS. Each black emission spectrum (measured before DNA displacement) has been scaled by the factor shown in the frame to allow clearer shape comparison with the red spectrum.

DNA interactions with SWCNTs depend on both base sequence and length. Among studied oligos with 12 bases, the data in Figure 2 show that the T_{12} ssDNA coating gave greatest deviation in UV absorption spectral fit. By contrast, nanotubes coated by C_{12}, which is composed of the other pyrimidine nucleotide, gave a spectrum closer to a combination of the separated components, implying much weaker π–π interactions with SWCNTs. It was not possible to make similar comparisons for DNA oligos composed of only purine bases (G or A) because those larger bases cannot uniformly adsorb onto the SWCNT surface.

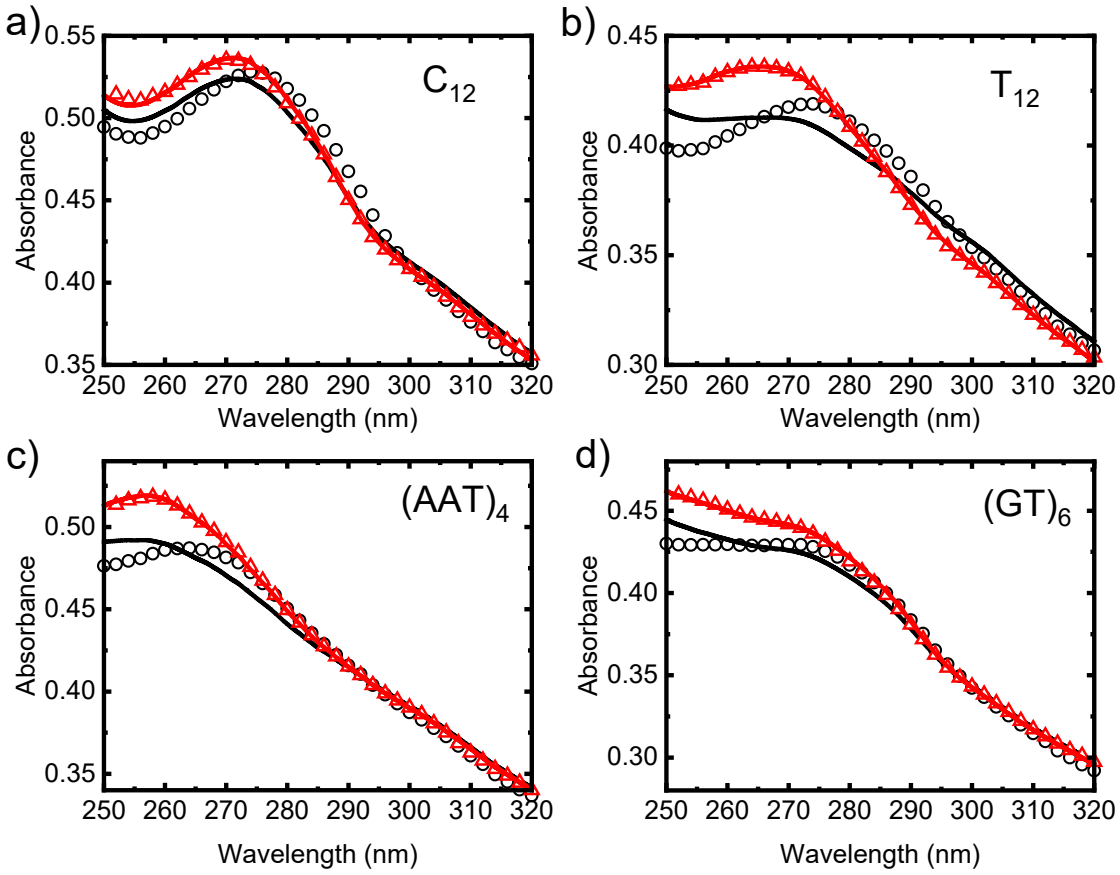

Figure 2. The UV absorption spectra of 195.1 HiPco SWCNT dispersions suspended by a) C_{12}, b) T_{12}, c) $(AAT)_4$, or d) $(GT)_6$ DNA oligos. Open symbols and solid curves show experimental data and best fits, respectively. Spectral fits are linear combinations of the spectra of free DNAs and SDS-suspended SWCNTs. Each panel shows spectra measured before (black circles) and after (red triangles) displacement of the DNA coating by added SDS.

Figure 3 displays UV absorption data related to the dependence of interactions on oligo length. Comparing Figure 2a with Figure 3a, we find that C_{30} induces stronger spectral perturbations than

C_{12}. This points to an increase in π–π interaction strength with length for this family of oligos. Less dependence on length was found from a comparison of spectra in T_{39} and T_{12}, possibly

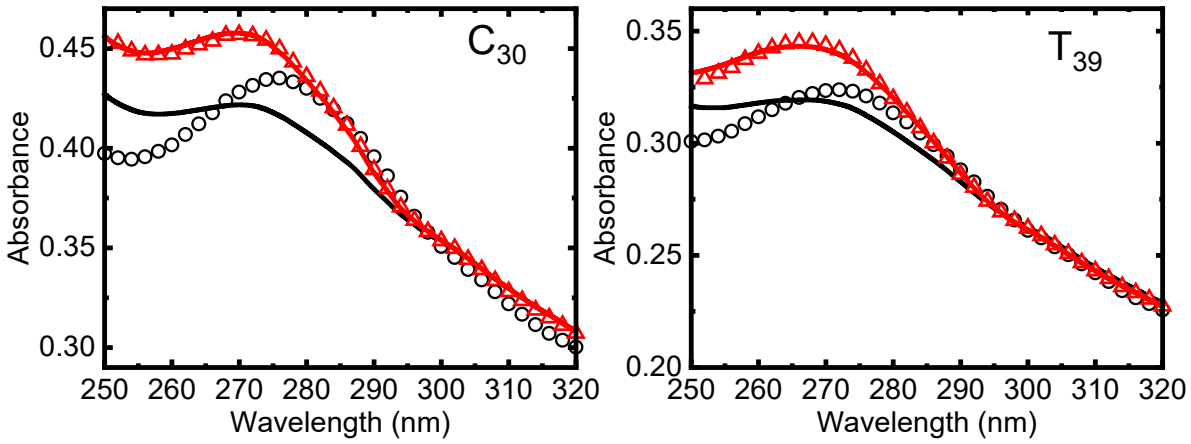

Figure 3. The UV absorption spectra of 195.1 HiPco SWCNT dispersions suspended by ssDNA oligos C_{30} (left frame), and T_{39} (right frame). Open symbols and solid curves show experimental data and best fits, respectively. Spectral fits are linear combinations of the spectra of free DNAs and SDS-suspended SWCNTs. Each panel shows spectra measured before (black circles and curves) and after (red triangles and curves) displacement of the DNA coating by added SDS.

because the perturbations were already substantial in the case of T_{12}.

We complemented our UV observations with fluorescence spectroscopy on the difference between interactions of SWCNTs with oligos containing only T or only C. Samples dispersed by T-containing ssDNA oligos gave much stronger fluorescence than those dispersed by C-containing oligos, even though their NIR absorption was lower. This suggests that the SWCNT surface was more completely covered by the T oligos than by the C oligos, as seems consistent with stronger overall interactions with the nanotube surface.

We determined the effective DNA/SWCNT mass ratios in dispersed nanotubes using the total masses of DNA and SWCNT found from UV spectral analysis. Table 1 shows the results for DNA and SWCNT concentrations and their ratios in each dispersion after dialysis to remove free DNA. A mass ratio of 1.17 was found for SWCNTs coated and suspended by the T_{12} and T_{39} ssDNA oligos, while the corresponding mass ratio was 1.06 for C_{12} and C_{30}. This difference in mass ratio may lead to the stronger UV spectral perturbations observed with thymine coatings as compared to cytosine coatings. We also found ssDNA/SWCNT mass ratios of approximately 1.11 and 0.87 for SWCNTs coated by oligos containing GT and AT nucleotides, respectively.

Table 1. Experimental Parameters for Dispersions of HiPco SWCNTs in Different ssDNA Oligos.

ssDNA oligo	DNA conc. (mg/L)	SWCNT conc. (mg/L)	DNA / SWCNT mass ratio	C atoms covered per DNA strand	C atoms covered per DNA base
T_{12}	3.03	2.58	1.17	255	21
T_{39}	2.28	1.95	1.16	845	22
C_{12}	3.23	3.04	1.06	267	22
C_{30}	2.77	2.64	1.05	684	23
$(GT)_6$ [1]	2.83	2.52	1.12	277	23
$(GT)_6$ [2]	4.61	4.20	1.10	284	24
$(AAAT)_3$	1.69	1.96	0.86	356	30
$(AAT)_4$	2.54	2.92	0.87	351	29

[1] sample prepared with a DNA / SWCNT mass ratio of 2
[2] sample prepared with a DNA / SWCNT mass ratio of 1

These observations are consistent with the general notion that adsorbed purine nucleotides occupy more SWCNT surface area than pyrimidine bases. For this reason, the mass of DNA needed to disperse SWCNTs tends to be lower for oligos that are richer in purines. Based on our experimental findings, we estimated the average number of carbon atoms covered per single DNA oligo and per DNA base of the oligo (see Table 1). The number of covered carbon atoms for oligos containing some purine bases was generally greater than for oligos containing only pyrimidine bases. Using the number of carbons covered per thymine nucleotide, we deduced the number of carbons covered per adenine and guanine. Figures 4a – 4d show MD simulation snapshots of the four relaxed DNA base monophosphates, each adsorbed on a graphene flake containing the experimentally deduced number of covered carbons. The simulations are consistent with our experimental findings that purine nucleotides cover more carbons than pyrimidine nucleotides. To further investigate DNA interactions with SWCNT surfaces, we performed MD simulations that were guided by the experimental DNA/SWCNT mass ratios.

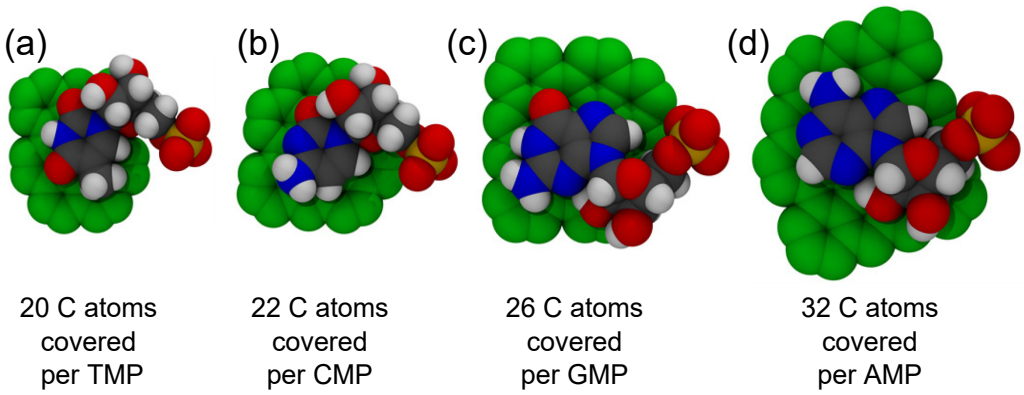

Figure 4. Experimentally-based molecular dynamics illustrations of the surface areas covered by adsorbed individual nucleotides: (a) thymidine monophosphate (TMP), (b) cytidine monophosphate (CMP), (c) guanosine monophosphate (GMP), and (d) adenosine monophosphate (AMP). Each monophosphate is shown on a graphene flake containing the number of covered carbon atoms deduced from SWCNT experiments. The graphene carbon atoms are drawn in green, while DNA carbon, oxygen, nitrogen, phosphorous, and hydrogen atoms are colored gray, red, blue, orange, and white, respectively.

Molecular dynamics simulations

We used our experimentally determined DNA/SWCNT mass ratios in constrained MD simulations that modeled the interactions of various ssDNA oligos with SWCNTs of different diameters. The experimental mass ratios were ensemble averages over a variety of SWCNT species with an average diameter near 0.9 nm. In our MD simulations, we used the (6,5), (7,6) and (8,7) SWCNT species to explore diameter-dependent effects in this range, but for each studied oligo, we applied the same DNA/SWCNT mass ratio with all three SWCNT species.

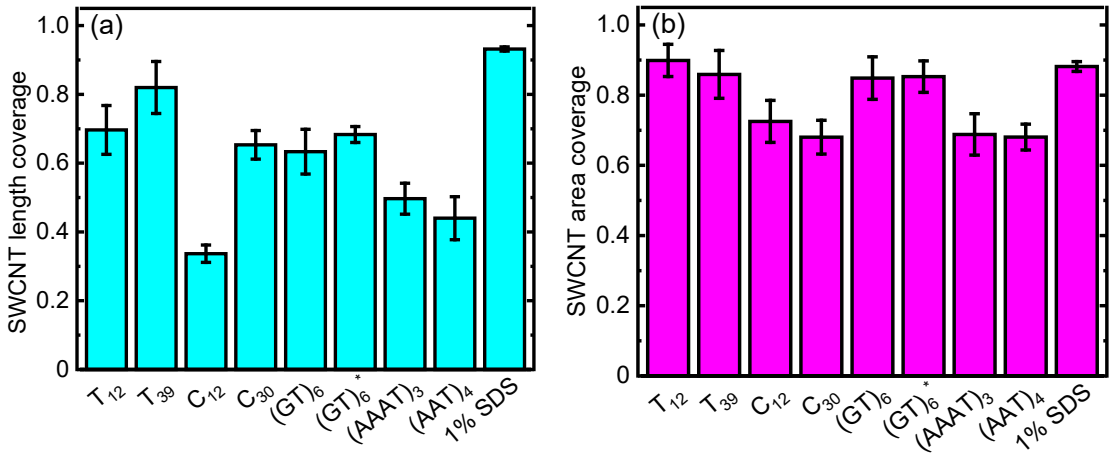

Figure 5. Computed coverage results from MD simulations of different ssDNA oligos wrapping (6,5), (7,6) or (8,7) SWCNTs. (a) The ensemble-averaged maximum axial lengths of three identical DNA strands adsorbed onto a SWCNT segment were summed and divided by the length of the segment to obtain the

plotted length coverage fractions. Separate values of those fractions are shown for eight labeled oligo compositions. (b) The ensemble-averaged ratios of covered-to-total SWCNT surface areas are plotted for the same set of simulations. Separate area coverage fractions are shown for the eight oligos. Values in both frames were averaged over MD simulations of three SWCNT species. Figure S4 includes detailed results for the separate SWCNT species. $(GT)_6$* denotes the SWCNT coated by $(GT)_6$ with a simulated DNA-to-SWCNT mass ratio of 1.

We computed two complementary coverage measures for SWCNT segments with adsorbed ssDNA: area and length coverages. For a given segment, area coverage is the fraction of SWCNT carbon atoms that are in close contact with ssDNA, whereas length coverage is the fraction of the segment's axial length that has adsorbed ssDNA. For a given area coverage, length coverage will be smaller for compact ssDNA morphologies than for extended ones. Figure 5 shows the oligo-dependent SWCNT length coverage and SWCNT area coverage, as averaged over the MD simulations results for the three SWCNT species. Figure S4 and Tables S1-S2 contain details on these calculated values. Among the oligos, those containing GT or only T showed the greatest SWCNT length and area coverages. Conversely, oligos containing AT or only C tended to show lower coverages. Simulations of SWCNTs coated by the surfactant sodium dodecyl sulfate (SDS) found comparatively greater length and area coverages, as seems to correspond to the higher fluorescence quantum yields (reflecting better isolation) observed for SWCNTs coated by SDS instead of ssDNA. Figure 6 shows snapshots from MD simulations of the studied systems, with the nanotube segment lengths chosen to agree with the experimental mass ratios. These snapshots illustrate that the incomplete SWCNT surface coverage arises mainly from gaps between adsorbed ssDNA strands or gaps between adsorbed SDS micellar clusters. The images also reveal greater circumferential coating inhomogeneity with ssDNA coatings as compared to SDS.

Our results point to the influence of nucleobase identity on ssDNA-SWCNT π–π interactions and the SWCNT PL emission intensity. For simplicity, we compare the DNA oligos composed of a single nucleotide (the poly-C and poly-T families). As shown in Figure 5, the poly-T oligos give greater SWCNT length coverage than the poly-C oligos. This implies that the poly-T oligos are more elongated along the SWCNT axis, interacting with more SWCNT carbon atom π-electrons and providing greater surface coverage than the poly-C oligos. We view this simulation finding as consistent with the stronger normalized PL emission and greater UV spectral perturbations observed for SWCNTs coated with poly-T as compared to poly-C oligos.

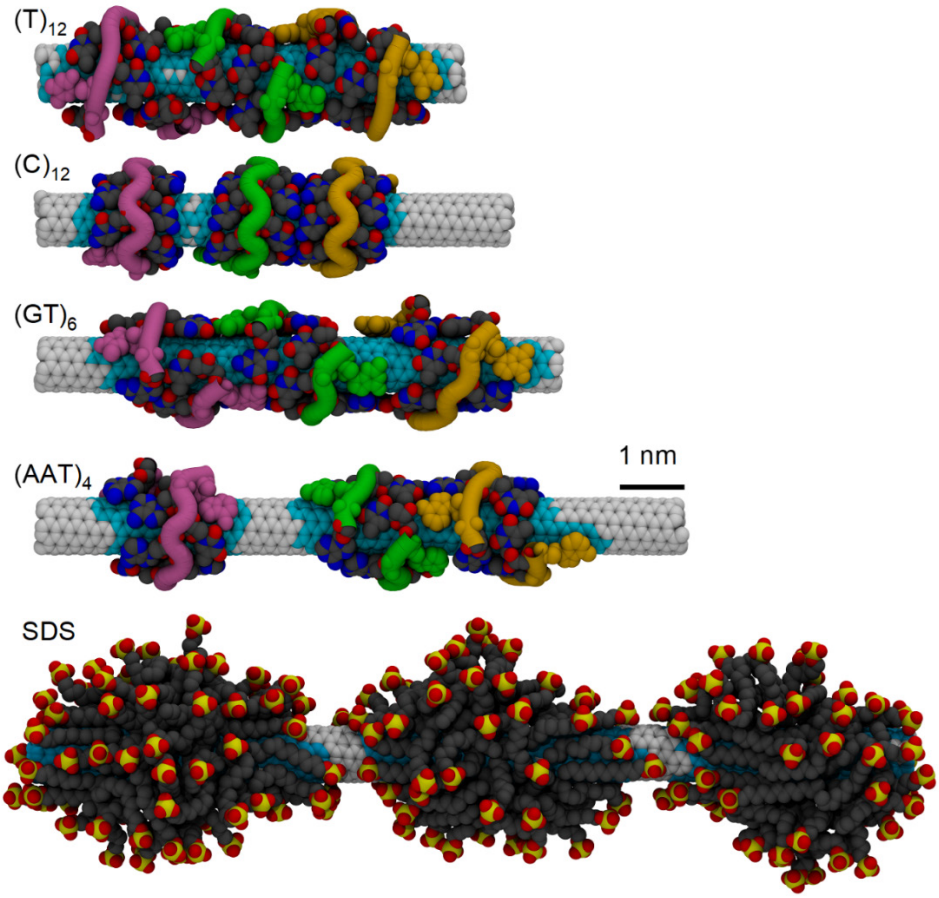

Figure 6. MD simulation snapshots of (6,5) SWCNTs wrapped by three ssDNA strands of each labeled oligo or by SDS surfactant above its critical micelle concentration. The SWCNT length in each MD simulation was chosen to give the experimental DNA-to-SWCNT ratio. To visualize the contacts between DNA strands and SWCNTs, all species are shown in van der Waals representation. DNA carbon, nitrogen, oxygen and sulfur atoms are shown in gray, blue, red, and yellow, respectively. The (6,5) SWCNT carbon atoms are drawn in white, and the cyan-colored SWCNT carbon atoms are covered by adsorbed species. To help distinguish the three different DNA strands, their backbones are shown in purple, green and orange. The correspondingly colored DNA bases are the groups of atoms that give maximum end-to-end axial coverage in the displayed snapshots.

We also performed MD simulations to investigate the effect of oligo length on ssDNA-SWCNT interactions for poly-T and poly-C oligos. Using the same experimentally-based DNA/SWCNT mass ratio for simulating C_{12}- and C_{30}-wrapped SWCNTs, we found equal SWCNT fractional surface area coverages but different length coverages. MD snapshots show that the C_{12} oligo assumes a much more compact structure on the SWCNT surface than does C_{30}, with the spatial arrangement of nucleobases constrained by the C_{30} backbone. As illustrated in Figure 6,

adsorbed C_{12} strands form ring structures that are distinct from the helical structures observed for C_{30} (see Figure S5). In the C_{12} rings, the ends of a single DNA strand meet and then become locked through hydrogen bonding of their DNA bases. By contrast, a helically wrapped DNA strand extends further along the nanotube axis and commonly shows a gap to a neighboring strand. The SWCNT length coverage by the ring-structured DNA strands is thus lower than for the helical strands, although both lead to equivalent SWCNT area coverage. Neither our MD simulations nor UV absorption spectra indicate significant differences between the wrapping of SWCNTs by T_{12} as compared to T_{39}. Figures 6 and S5 present snapshots of those two poly-T oligos adsorbed on a (6,5) SWCNT segment.

Correlation between computational and experimental results

Our experiments and simulations both indicate that adsorbed poly-T ssDNA oligos have stronger interactions with SWCNT surfaces than do poly-C oligos. Tables 1 and S2 list the experimental and computed values for the SWCNT surface coverage of several different oligos. As shown in Figure S6, there is a good correlation between these results, although the simulation coverages fall systematically below the experimental values. We note that DNA oligos do not cover SWCNT surfaces as completely as surfactants such as SDS. This view is supported by previous studies,[44,45] and by our observations that the fluorescence peaks from DNA-dispersed SWCNTs are weaker and broader than from surfactant-coated SWCNTs.[18,37]

We hypothesize that relative fluorescence yields can be used to compare surface coverages among ssDNA-coated SWCNTs. Table S3 shows the spectrally integrated near-IR fluorescence emission intensity, normalized to total near-IR absorption, for different SWCNT dispersions. The values indicate that SWCNTs coated by poly-C oligos have the lowest emission yields. For comparison, we also measured the emission yield and computationally investigated the morphology and surface coverages of SDS surfactant coatings on (6,5), (7,6) and (8,7) SWCNTs at concentrations above the critical micelle concentration. Figure S7 shows how the emission yields correlate with the simulation values for SWCNT length coverage and surface coverage. In this graph, each symbol area is proportional to the experimental emission yield for SWCNTs in a specific coating and the x and y coordinates of that symbol are the values from Figures 5a and 5b respectively. Symbols representing poly-C, poly-T, and GT-containing oligos show the hypothesized positive correlation between emission yields and SWCNT coverages. The exception

is the $(AAAT)_3$ oligo, which is a clear outlier with a higher emission yield than would be predicted from the simulated coverages.

We suggest that $(AAAT)_3$ is anomalous because its two ends can form hydrogen bonds between the adenosine and thymidine nucleotides, which are complementary in DNA hybridization. To investigate this possibility, we used MD simulation data for all studied oligos to calculate ensemble averages of the total number of hydrogen bonds per base and the total number of hydrogen bonds per strand connecting the two ends. Both values were averaged over the three representative SWCNT species. Although the results, shown in Figure S8a, indicate that DNA bases within AT-containing DNA oligos form fewer hydrogen bonds than most other DNA oligos, Figure S8b shows that their ends are hydrogen bonded more than for other DNA oligos. This effect may have led to kinetic trapping in the MD simulations and then inadequate sampling of the adsorbed DNA conformations, which can cause poor agreement between experiments and simulations. Additionally, Figure S8a shows that poly-C oligos contain the greatest number of hydrogen bonds per DNA base. This seems consistent with our finding that they assume the most compact structures, leading to low SWCNT surface area coverage and low fluorescence yields. Although hydrogen bonding may make the simulated conformations prone to kinetic trapping, we are confident that the poly-C structures formed in our standard MD simulations are realistic, as previous REMD simulations also found similar compact structures of C_{12} adsorbed on SWCNTs.[29]

Our MD simulations indicate that SWCNT coverage is diameter dependent, with a systematic SWCNT area coverage trend of (6,5) < (7,6) < (8,7) for all studied DNA coatings (Figure S4). This finding agrees with our previous MD study of a single oligo, which found more complete surface coverage for larger diameter SWCNTs.[45] MD simulation snapshots corresponding to the surface area coverage results quantified in Figure S4 and Tables S1 and S2 are shown for (6,5), (7,6), and (8,7) SWCNTs in Figures 6, S9 and S10, respectively.

CONCLUSIONS

We spectroscopically measured ssDNA/SWCNT mass ratios ranging from 1.17 to 0.86 for a SWCNT HiPco batch dispersed in either poly-T, poly-C, GT-containing, or AT-containing ssDNA oligos. From the measured DNA/SWCNT mass ratios, we estimate that a single adsorbed thymine, cytosine, adenine, or guanine nucleotide covers an average of 20, 22, 26, or 32 carbon atoms, respectively, on the SWCNT surface. Additionally, UV absorption spectroscopy of DNA-

dispersed SWCNTs revealed the effects of DNA oligo composition and length on their electronic interactions with SWCNTs. We deduced that short poly-T DNA oligos have stronger π–π stacking interactions with SWCNT surfaces than short poly-C DNA oligos, while both long poly-C and poly-T DNA oligos have strong interactions. We subsequently performed MD simulations constrained by the experimentally determined DNA/SWCNT mass ratios, and compared the SWCNT surface area coverages found for different DNA oligos to each other and to SDS-coated SWCNTs. The results suggest that poly-T and GT-containing DNA oligos give the greatest SWCNT surface coverage, as is consistent with the observation that they also had the greatest fluorescence yields. However, $(AAAT)_3$-DNA dispersed SWCNT was an outlier, showing a fluorescence yield as strong as poly-T and GT-containing DNA dispersed SWCNTs, even though its SWCNT coverage in MD simulations was lower than for those two DNA oligo families. We suggest that this exception may reflect hydrogen bond formation between the two complementary ends of $(AAAT)_3$ strands, which might restrict the simulated structural dynamics of this DNA oligo on SWCNT surfaces.

ASSOCIATED CONTENT

Supporting Information. Additional absorption spectra of SWCNTs in ssDNA before and after displacement; plots and tables with MD simulation results; images of MD structural snapshots for ssDNA oligos adsorbed on (6,5), (7,6), and (8,7) SWCNT segments; correlation plots for SWCNT surface coverages and fluorescence intensity; hydrogen bonding analyses of MD structures.

AUTHOR INFORMATION

Corresponding Author

* E-mail: weisman@rice.edu

Present Address

§ A.A.A.: Massachusetts Institute of Technology, Cambridge, MA 02139, United States

ORCID

Ali A. Alizadehmojarad: 0000-0001-6806-5415

Sergei M. Bachilo: 0000-0001-5236-1383

R. Bruce Weisman: 0000-0001-8546-9980

NOTES

R.B.W. has a financial interest in Applied NanoFluorescence, LLC, which manufactures one of the instruments used in this study.

ACKNOWLEDGMENTS

This research was supported by a grant from the National Science Foundation (CHE-2203309).

REFERENCES

(1) Dresselhaus, M. S.; Dresselhaus, G.; Avouris, Ph. *Carbon Nanotubes: Synthesis, Structure, Properties, and Applications*; Topics in Applied Physics; Springer-Verlag: New York, 2001; Vol. 80.

(2) Reich, S.; Thomsen, C.; Maultzsch, J. *Carbon Nanotubes: Basic Concepts and Physical Properties*; Wiley-VCH: Weinheim, 2004.

(3) O'Connell, M. J.; Bachilo, S. M.; Huffman, C. B.; Moore, V. C.; Strano, M. S.; Haroz, E. H.; Rialon, K. L.; Boul, P. J.; Noon, W. H.; Kittrell; et al. Band Gap Fluorescence from Individual Single-Walled Carbon Nanotubes. *Science* **2002**, *297* (5581), 593–596. https://doi.org/10.1126/science.1072631.

(4) Moore, V. C.; Strano, M. S.; Haroz, E. H.; Hauge, R. H.; Smalley, R. E. Individually Suspended Single-Walled Carbon Nanotubes in Various Surfactants. *Nano Lett.* **2003**, *3*, 1379–1382.

(5) Khripin, C. Y.; Manohar, S.; Zheng, M.; Jagota, A. Measurement of Electrostatic Properties of DNA-Carbon Nanotube Hybrids by Capillary Electrophoresis. *J. Phys. Chem. C* **2009**, *113* (31), 13616–13621. https://doi.org/10.1021/jp903197d.

(6) Shastry, T. A.; Morris-Cohen, A. J.; Weiss, E. A.; Hersam, M. C. Probing Carbon Nanotube-Surfactant Interactions with Two-Dimensional DOSY NMR. *J. Am. Chem. Soc.* **2013**, *135* (18), 6750–6753.

(7) Fagan, J. A.; Zheng, M.; Rastogi, V.; Simpson, J. R.; Khripin, C. Y.; Silvera Batista, C. A.; Hight Walker, A. R. Analyzing Surfactant Structures on Length and Chirality Resolved (6,5) Single-Wall Carbon Nanotubes by Analytical Ultracentrifugation. *ACS Nano* **2013**, *7* (4), 3373–3387.

(8) Arnold, M. S.; Suntivich, J.; Stupp, S. I.; Hersam, M. C. Hydrodynamic Characterization of Surfactant Encapsulated Carbon Nanotubes Using an Analytical Ultracentrifuge. *ACS Nano* **2008**, *2* (11), 2291–2300.

(9) Alizadehmojarad, A. A.; Bachilo, S. M.; Kolomeisky, A. B.; Weisman, R. B. Morphology Transitions of SDS Coatings on Single-Walled Carbon Nanotubes. *J. Phys. Chem. C* **2024**, *128* (14), 6126–6132. https://doi.org/10.1021/acs.jpcc.4c00482.

(10) Roxbury, D.; Mittal, J.; Jagota, A. Molecular-Basis of Single-Walled Carbon Nanotube Recognition by Single-Stranded DNA. *Nano Lett.* **2012**, *12* (3), 1464–1469. https://doi.org/10.1021/nl204182b.

(11) Beyene, A. G.; Alizadehmojarad, A. A.; Dorlhiac, G.; Goh, N.; Streets, A. M.; Král, P.; Vuković, L.; Landry, M. P. Ultralarge Modulation of Fluorescence by Neuromodulators in Carbon Nanotubes Functionalized with Self-Assembled Oligonucleotide Rings. *Nano Lett.* **2018**, *18* (11), 6995–7003. https://doi.org/10.1021/acs.nanolett.8b02937.

(12) Shankar, A.; Zheng, M.; Jagota, A. Energetic Basis of Single-Wall Carbon Nanotube Enantiomer Recognition by Single-Stranded DNA. *J. Phys. Chem. C* **2017**, *121* (32), 17479–17487. https://doi.org/10.1021/acs.jpcc.7b05168.

(13) Roxbury, D.; Jagota, A.; Mittal, J. Structural Characteristics of Oligomeric DNA Strands Adsorbed onto Single-Walled Carbon Nanotubes. *J. Phys. Chem. B* **2013**, *117* (1), 132–140. https://doi.org/10.1021/jp309523a.

(14) Xhyliu, F.; Ao, G. Chirality-Pure Carbon Nanotubes Show Distinct Complexation with Recognition DNA Sequences. *Carbon* **2020**, *167*, 601–608. https://doi.org/10.1016/j.carbon.2020.06.040.

(15) Shankar, A.; Mittal, J.; Jagota, A. Binding between DNA and Carbon Nanotubes Strongly Depends upon Sequence and Chirality. *Langmuir* **2014**, *30* (11), 3176–3183. https://doi.org/10.1021/la500013c.

(16) Zheng, M.; Jagota, A.; Semke, E. D.; Diner, B. A.; McClean, R. S.; Lustig, S. R.; Richardson, R. E.; Tassi, N. G. DNA-Assisted Dispersion and Separation of Carbon Nanotubes. *Nat. Mater.* **2003**, *2*, 338–342.

(17) Zheng, M.; Jagota, A.; Strano, M. S.; Santos, A. P.; Barone, P.; Chou, S. G.; Diner, B. A.; Dresselhaus, M. S.; McLean, R. S.; Onoa, G. B.; et al. Structure-Based Carbon Nanotube Sorting by Sequence-Dependent DNA Assembly. *Science* **2003**, *302* (5650), 1545–1548.

(18) Lei, K.; Bachilo, S. M.; Weisman, R. B. Kinetics of Single-Wall Carbon Nanotube Coating Displacement by Single-Stranded DNA Depends on Nanotube Structure. *ACS Nano* **2023**, *17* (17), 17568–17575. https://doi.org/10.1021/acsnano.3c06906.

(19) Ao, G.; Streit, J. K.; Fagan, J. A.; Zheng, M. Differentiating Left- and Right-Handed Carbon Nanotubes by DNA. *J. Am. Chem. Soc.* **2016**, *138* (51), 16677–16685. https://doi.org/10.1021/jacs.6b09135.

(20) Ao, G.; Khripin, C. Y.; Zheng, M. DNA-Controlled Partition of Carbon Nanotubes in Polymer Aqueous Two-Phase Systems. *J. Am. Chem. Soc.* **2014**, *136* (29), 10383–10392. https://doi.org/10.1021/ja504078b.

(21) Manohar, S.; Mantz, A. R.; Bancroft, K. E.; Hui, C.-Y.; Jagota, A.; Vezenov, D. V. Peeling Single-Stranded DNA from Graphite Surface to Determine Oligonucleotide Binding Energy by Force Spectroscopy. *Nano Lett.* **2008**, *8* (12), 4365–4372. https://doi.org/10.1021/nl8022143.

(22) Strano, M. S.; Zheng, M.; Jagota, A.; Onoa, G. B.; Heller, D. A.; Barone, P. W.; Usrey, M. L. Understanding the Nature of the DNA-Assisted Separation of Single-Walled Carbon Nanotubes Using Fluorescence and Raman Spectroscopy. *Nano Lett.* **2004**, *4*, 543–550.

(23) Tu, X. M.; Zheng, M. A DNA-Based Approach to the Carbon Nanotube Sorting Problem. *Nano Res.* **2008**, *1* (3), 185–194.

(24) Tu, X.; Manohar, A.; Jagota, A.; Zheng, M. DNA Sequence Motifs for Structure-Specific Recognition and Separation of Carbon Nanotubes. *Nature* **2009**, *460*, 250–253.

(25) Ao, G.; Khripin, C. Y.; Zheng, M. DNA-Controlled Partition of Carbon Nanotubes in Polymer Aqueous Two-Phase Systems. *J. Am. Chem. Soc.* **2014**, *136* (29), 10383–10392. https://doi.org/10.1021/ja504078b.

(26) Alizadehmojarad, A. A.; Bachilo, S. M.; Weisman, R. B. Compositional Analysis of ssDNA-Coated Single-Wall Carbon Nanotubes through UV Absorption Spectroscopy. *Nano Lett.* **2022**, *22* (20), 8203–8209. https://doi.org/10.1021/acs.nanolett.2c02850.

(27) Johnson, R. R.; Kohlmeyer, A.; Johnson, A. T. C.; Klein, M. L. Free Energy Landscape of a DNA - Carbon Nanotube Hybrid Using Replica Exchange Molecular Dynamics. *Nano Lett.* **2009**, *9* (2), 537–541. https://doi.org/10.1021/n1802645d.

(28) Johnson, R. R.; Johnson, A. T. C.; Klein, M. L. Probing the Structure of DNA−Carbon Nanotube Hybrids with Molecular Dynamics. *Nano Lett.* **2008**, *8* (1), 69–75. https://doi.org/10.1021/nl071909j.

(29) Alizadehmojarad, A. A.; Zhou, X.; Beyene, A. G.; Chacon, K. E.; Sung, Y.; Pinals, R. L.; Landry, M. P.; Vuković, L. Binding Affinity and Conformational Preferences Influence Kinetic Stability of Short Oligonucleotides on Carbon Nanotubes. *Adv. Mater. Interfaces* **2020**, *7* (15), 2000353. https://doi.org/10.1002/admi.202000353.

(30) Lin, Z.; Yang, Y.; Jagota, A.; Zheng, M. Machine Learning-Guided Systematic Search of DNA Sequences for Sorting Carbon Nanotubes. *ACS Nano* **2022**, *16* (3), 4705–4713. https://doi.org/10.1021/acsnano.1c11448.

(31) Miyauchi, Y.; Saito, R.; Sato, K.; Ohno, Y.; Iwasaki, S.; Mizutani, T.; Jiang, J.; Maruyama, S. Dependence of Exciton Transition Energy of Single-Walled Carbon Nanotubes on Surrounding Dielectric Materials. *Chem. Phys. Lett.* **2007**, *442* (4–6), 394–399. https://doi.org/10.1016/j.cplett.2007.06.018.

(32) Weisman, R. B. Fluorimetric Characterization of Single-Walled Carbon Nanotubes. *Anal. Bioanal. Chem.* **2010**, *396* (3), 1015–1023.

(33) Rocha, J. D.; Bachilo, S. M.; Ghosh, S.; Arepalli, S.; Weisman, R. B. Efficient Spectrofluorimetric Analysis of Single-Walled Carbon Nanotube Samples. *Anal. Chem.* **2011**, *83* (19), 7431–7437.

(34) Hart, K.; Foloppe, N.; Baker, C. M.; Denning, E. J.; Nilsson, L.; MacKerell, A. D. Optimization of the CHARMM Additive Force Field for DNA: Improved Treatment of the Bi/Bii Conformational Equilibrium. *J. Chem. Theory Comput.* **2012**, *8* (1), 348–362. https://doi.org/10.1021/ct200723y.

(35) Phillips, J. C.; Braun, R.; Wang, W.; Gumbart, J.; Tajkhorshid, E.; Villa, E.; Chipot, C.; Skeel, R. D.; Kalé, L.; Schulten, K. Scalable Molecular Dynamics with NAMD. *J. Comput. Chem.* **2005**, *26* (16), 1781–1802. https://doi.org/10.1002/jcc.20289.

(36) Darden, T.; York, D.; Pedersen, L. Particle Mesh Ewald: An Nlog(N) Method for Ewald Sums in Large Systems. *J. Chem. Phys.* **1993**, *98* (12), 10089–10092. https://doi.org/10.1063/1.464397.

(37) Lei, K.; Bachilo, S. M.; Weisman, R. B. Diameter-Dependent Competitive Adsorption of Sodium Dodecyl Sulfate and Single-Stranded DNA on Carbon Nanotubes. *J. Phys. Chem. Lett.* **2023**, *14* (49), 11043–11049.

(38) Sims, C. M.; Fagan, J. A. Surfactant Chemistry and Polymer Choice Affect Single-Wall Carbon Nanotube Extraction Conditions in Aqueous Two-Polymer Phase Extraction. *Carbon* **2022**, *191*, 215–226. https://doi.org/10.1016/j.carbon.2022.01.062.

(39) Roxbury, D.; Tu, X.; Zheng, M.; Jagota, A. Recognition Ability of DNA for Carbon Nanotubes Correlates with Their Binding Affinity. *Langmuir* **2011**, *27* (13), 8282–8293. https://doi.org/10.1021/la2007793.

(40) Shankar, A.; Mittal, J.; Jagota, A. Binding between DNA and Carbon Nanotubes Strongly Depends upon Sequence and Chirality. *Langmuir* **2014**, *30* (11), 3176–3183. https://doi.org/10.1021/la500013c.

(41) Zheng, Y.; Bachilo, S. M.; Weisman, R. B. Enantiomers of Single-Wall Carbon Nanotubes Show Distinct Coating Displacement Kinetics. *J. Phys. Chem. Lett.* **2018**, *9* (13), 3793–3797. https://doi.org/10.1021/acs.jpclett.8b01683.

(42) Jena, P. V.; Safaee, M. M.; Heller, D. A.; Roxbury, D. DNA-Carbon Nanotube Complexation Affinity and Photoluminescence Modulation Are Independent. *ACS Appl. Mater. Interfaces* **2017**, *9* (25), 21397–21405. https://doi.org/10.1021/acsami.7b05678.

(43) Yang, Y.; Sharma, A.; Noetinger, G.; Zheng, M.; Jagota, A. Pathway-Dependent Structures of DNA-Wrapped Carbon Nanotubes: Direct Sonication vs Surfactant/DNA Exchange. *J. Phys. Chem. C* **2020**, *124* (16), 9045–9055.

(44) Jeng, E. S.; Moll, A. E.; Roy, A. C.; Gastala, J. B.; Strano, M. S. Detection of DNA Hybridization Using the Near-Infrared Band-Gap Fluorescence of Single-Walled Carbon Nanotubes. *Nano Lett.* **2006**, *6* (3), 371–375. https://doi.org/10.1021/nl051829k.

(45) Zheng, Y.; Alizadehmojarad, A. A.; Bachilo, S. M.; Kolomeisky, A. B.; Weisman, R. B. Dye Quenching of Carbon Nanotube Fluorescence Reveals Structure-Selective Coating Coverage. *ACS Nano* **2020**, *14* (9), 12148–12158. https://doi.org/10.1021/acsnano.0c05720.

Table of Contents Figure